Icarus 219 (2012) 498–501

Contents lists available at SciVerse ScienceDirect

Icarus

journal homepage: www.elsevier.com/locate/icarus

Note

The electromagnetic pickup of submicron-sized dust above Enceladus's northern hemisphere

William M. Farrell [a,*], Jan-Erik Wahlund [b], Michiko Morooka [b], Donald A. Gurnett [c], William S. Kurth [c], Robert J. MacDowall [a]

[a] NASA/Goddard SFC, Greenbelt, MD 21044, United States
[b] Swedish Inst. of Space Physics, Uppsala, Sweden
[c] University of Iowa, Iowa City, IA 52242, United States

ARTICLE INFO

Article history:
Received 7 July 2011
Revised 31 January 2012
Accepted 26 February 2012
Available online 14 March 2012

Keywords:
Saturn
Saturn, satellites
Saturn, magnetosphere
Enceladus

ABSTRACT

As the saturnian magnetoplasma sweeps past Enceladus, it experiences both a decrease in electron content and sharp slowdown in the northern hemisphere region within ~5 Enceladus Radii (R_e). This slowdown is observed by Cassini in regions not obviously associated with the southern directed plume-originating ions. We suggest herein that the decrease in northern hemisphere electron content and plasma slowdown could both be related to the presence of fine dust grains that are being accelerated by the Lorentz force created within the saturnian magnetic field system.

Published by Elsevier Inc.

1. Introduction

On 12 March 2008, the Cassini spacecraft made a close approach to the active moon Enceladus, on a trajectory passing by the body from northern regions into southern regions, ultimately to be immersed in the active south polar jet material (Porco et al., 2006; Waite et al., 2006, 2009). Fig. 1 (inset) shows the trajectory of the spacecraft in an Enceladus frame of reference where $+x$ is oriented in the direction of the moon's orbital velocity (out of the plane of the paper), $+y$ is oriented towards Saturn, and $+z$ is oriented out of the moon's orbital plane. The southern hemisphere plume is illustrated in the figure as the purple-shaded region approximately indicating the location of highest gas and dust activity (Waite et al., 2006; Spahn et al., 2006a). The spacecraft moved primarily southward at ~14 km/s, passing near the plume jets. The Enceladus' radius is ~250 km and thus the entire encounter lasted on the order of 10 min. The magnetic field is oriented almost due south (along $-z$).

While the southern hemisphere portion of the transit containing the plume garners great interest, the northern hemisphere portion of the transit also had unexpected activity as observed by Cassini's Radio and Plasma Wave System (RPWS) (Gurnett et al., 2004), the Langmuir Probe component of the RPWS (Wahlund et al., 2005), and Cassini Plasma Spectrometer (CAPS) (Young et al., 2004; Tokar et al., 2009). Specifically, in the northern hemisphere within $5R_e$ of the body (just before 19:05:00 SCET in Fig. 1), the ambient corotating plasma experienced a clear and distinct electron density dropout as evident by a sharp decrease in the plasma wave upper hybrid resonance frequency (Farrell et al., 2009, 2010), as evident in the Cassini CAPS electron spectrometer (Tokar et al., 2009) and in the electron density measured directly via the Langmuir Probe (Wahlund et al., 2009; Shafiq et al., 2011; Morooka et al., 2011). The upper hybrid resonance frequency is functionally dependent on the square root of the electron charge density, $\rho_e^{1/2}$, and thus can be used to derive an electron concentration value (Farrell et al., 2009). The electron concentration decreased precipitously starting just before 19:05:00 SCET and remained below the ion density, ρ_i, for the next 10 min. The ratio of ρ_i/ρ_e was as large as ~30 even within the plume region (~19:07 SCET) where ionization was enhanced. We focus herein on the northern hemisphere observations.

The commencement of the electron dropout in the northern hemisphere occurred well away from the south polar plume, when the spacecraft was azimuthally-displaced almost $2R_e$ away from the Enceladus fluxtube, but also occurred at a time when RPWS was registering an increasingly-large number of micron-sized dust impacts (see Figs. 1 and 2 of Farrell et al. (2010)). Possible mechanisms to explain the electron dropout were considered previously (Farrell et al., 2009): (1) Loss rates from water ion–electron recombination were found to be a factor of 10^4 to low to explain the electron depletion. (2) Electron dissociative attachment of H_2O also had loss rates orders of magnitude below than required to explain the severe northern hemisphere electron loss. However, the spacecraft/dust impact rate exceed 20 per second for >2 μm grain sizes during the electron dropout period. It was concluded that small particulates could be the source of the strong loss/absorption of plasma electrons; the dust thus becoming the dominant negative charge carrier. Shafiq et al. (2011) derived dust concentrations assuming that the dust-plasma system maintains neutrality such that $\rho_i + \rho_e + \rho_d = 0$ where ρ_d is the dust charge density with $|\rho_d| > |\rho_e|$. They found that the inclusion of a large population of submicron dust grains (<300 nm) in equilibrium with the local plasma could best account for loss of electrons.

Just before 19:05 SCET while Cassini was in the northern hemisphere, the ambient saturnian plasma underwent a clear and distinct decrease in velocity, dropping from ~30 km/s to well below 10 km/s (in Saturn's frame of reference) within 90 s (Tokar et al., 2009; Farrell et al., 2010; Morooka et al., 2011). While a significant velocity decrease is anticipated after 19:06:30 SCET in the southern hemisphere in association with the electromagnetic pickup of plume ions (Tokar et al., 2006, 2009; Pontius and Hill, 2006), the velocity decrease is observed to commence nearly 90 s earlier than anticipated. The cause of the premature slow down of the northern convecting plasma was not initially obvious. However, the coincidence of the

* Corresponding author. Fax: +1 301 286 3346.
E-mail address: william.m.farrell@nasa.gov (W.M. Farrell).

0019-1035/$ - see front matter Published by Elsevier Inc.
doi:10.1016/j.icarus.2012.02.033

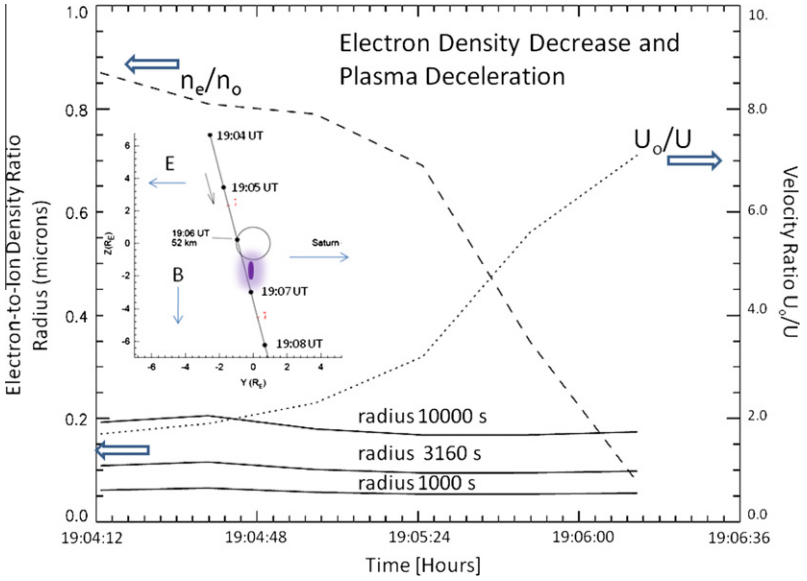

Fig. 1. Electron-to-ion density ratio, nominal-to-measured flow speed and calculated pickup grain radius for lifetimes of 10,000, 3160 and 1000 s during the Cassini northern hemisphere inbound E3 passage. The inset shows the Cassini trajectory in Enceladus co-rotation coordinates. At closest approach, the spacecraft passed slightly in front of the moon, in the positive +*X* direction.

distinct electron dropout in cadence with the sharp plasma slow down suggests that the two are intimately linked.

It was suggested (Farrell et al., 2010) that dust is picked-up by the corotating magnetic field and mass loaded onto field lines about the moon. The same submicron grains suspected to be present based on charge conservation arguments (Shafiq et al., 2011) will also be susceptible to Lorentz forces. We demonstrate herein that pickup currents from submicron sized dust are a likely candidate to account for both the simultaneous electron dropout and reduction of the plasma flow speed. In essence we infer the presence of the northern hemisphere dust by its behavior on the plasma.

2. Dust acceleration

The acceleration of dust in the magnetoplasma environment is defined by the Lorentz force, $\mathbf{F} = q(\mathbf{E} + \mathbf{v} \times \mathbf{B})$, where E is the electric field, v is the relative velocity between the grain and the convecting magnetic field, B. Table 1 lists expected grain characteristics in the near-Enceladus region, assuming the negatively-charged grains are in equilibrium with the plasma (near −10 V). As indicated in the table, the coupling coefficient to electromagnetic forces, q/m, increases with decreasing grain radius (varying as $q/m \sim r^{-2}$). As such, grains below 300 nm are intimately coupled to the ambient electromagnetic environment, especially when compared to micron-sized grains. Table 1 also lists the accelerations on dust grains near Enceladus by the moon's gravity, Saturn's gravity, corotation E-field, and magnetic force. Acceleration from Saturn, a_{Sat}, is the acceleration ($\sim v_E^2/r$) associated with Keplerian orbital motion.

Consider the southward-directed south pole plume emission: Charged grains from the plume are ejected on ballistic trajectories at speeds ranging from 10's to many 100's of meters per second (Porco et al., 2006). The grain mass determines the final outcome for the trajectories. Micron sized particles are predominately influenced by the gravity wells of the moon and Saturn. Kempf et al. (2010) demonstrated via dynamic particle tracing that grains from the fissures ejected near 250 m/s are capable of complex motion including trajectories that allow excursions well into the northern hemispheres. The modeling is consistent with Cassini dust analyzer (Kempft et al., 2008, 2010) and RPWS dust (Farrell et al., 2010) observations of an overall north–south dust envelop that extends ~20R_e above and below the orbital plane. They also demonstrated that a substantial amount of icy-dust falls back to the surface, coating the southern hemisphere and large portions of the northern hemisphere. However, for grains less than 300 nm, the effect of Lorentz forces will have the dominant influence on particle dynamics consistent with the large q/m value listed in Table 1.

For example, a negatively charged 100 nm particle released at 500 m/s will feel the ambient E-field in the $-Y$ direction as the dominant force. This force will accelerate the grain radially-inward toward Saturn. However, as the particulate's velocity increases along the Enceladus–Saturn radial direction, the trajectory will start to curve azimuthally (in the plasma corotating +*X* direction) via the magnetic $v \times B$ force. At 3 km/s the $v \times B$ force on the 0.1 μm grain is 12% that of E, but as acceleration increases, the magnitude of vB becomes comparable to E. Effectively, the par-

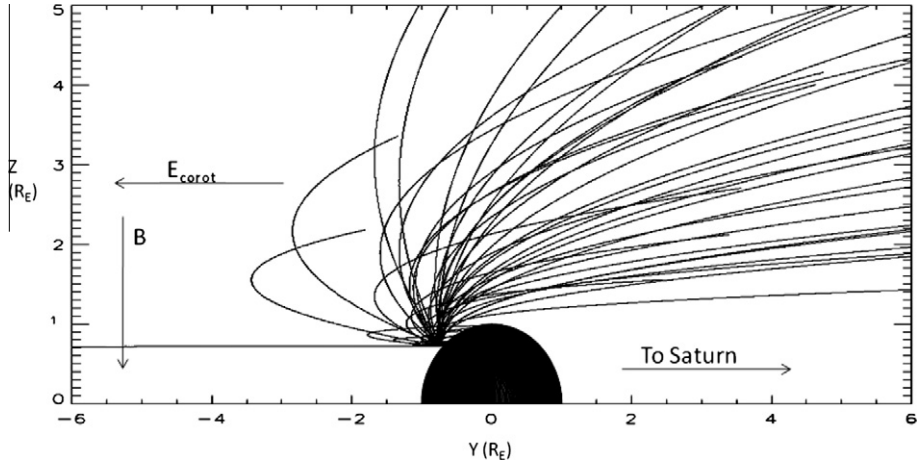

Fig. 2. A Monte Carlo demonstration of the impact ejecta trajectory from a localized position in the northern latitude after 2000 s. The negatively-charged submicron grains near 100 nm get accelerated by E.

Table 1
The mass, M, equilibrium charge, Q, and expected particulate accelerations, a, associated with grains of various sizes in the near-Enceladus environment. Charge is calculated assuming a −10 V potential on the grains. The acceleration, a_{moon}, at the moon is that at the surface. Accelerations from the corotation E-field strongly influence the submicron particle dynamics.

	30 nm	100 nm	300 nm	1000 nm
Mass (kg)	10^{-19}	4×10^{-18}	10^{-16}	4×10^{-15}
Q (fC)	−0.12	−0.4	−1.2	−4
$\|Q/M\|$	1200	100	12	1
a_{moon} (m/s^2)	0.1	0.1	0.1	0.1
a_{Saturn} (m/s^2)	0.6	0.6	0.6	0.6
a_E (m/s^2)	9.6	0.8	0.1	8×10^{-3}
$a_{vB\ @\ 3km/s}$ (m/s^2)	1.1	0.1	10^{-2}	10^{-3}

ticle is being picked-up by the magnetic field, with the electric field as the driving force in accelerating the grain from initially slow to fast velocities.

Analogous to Goertz (1980), the negatively-charged submicron particle acceleration occurs in a direction opposite to the co-rotational E-field. This dust-created 'pick-up' current then acts to apply a $J_\perp \times B$ force in the inner magnetosphere that correspondingly creates a drag force on the collisionally-driven ionosphere (Hill, 1979; Pontius and Hill, 1982). From a kinetic point of view, the perpendicular dust current is associated with a finite cross-magnetic field conductivity that creates a shielding E-field, effectively slowing the plasma down in the region where $J_\perp$ is present. The force on the flux tube from the pick-up current is:

$$F_x = (J_y \times B_z)_x = \rho_d v_d B_z = (\rho_d q_d \tau / m_d) E_y B_z \quad (1)$$

where ρ_d is the dust charge density, v_d, is the dust speed in the Y direction associated with motion under driving acceleration $q_d E_y/m_d$ which has been operating over the grain lifetime of τ. The quantity B_z is the southward directed B-field near 320 nT. The finite-valued conductivity perpendicular to the magnetic field associated with $J_\perp$ is $\sigma_d = \rho_d q_d \tau / m_d$. The dust conductance is $\Sigma_d = \sigma_d L_z$, where L_z is the length of this finite conductivity region along the magnetic field lines ($\sim 3R_e$). We note that E_y applied in Eq (1) is not the full value of the co-rotational field, E_o but instead that E-field self-consistently reduced by the dust current shielding effects. This shielding effect results from the physical displacement of the negatively-charged dust that creates a polarization E that offsets the full co-rotation E. This reduced shielded E then slows the plasma ion flow in the X-direction (i.e., $v_x^{reduced}$ is equal to $E_y^{shielded}/B_z$).

Given that the submicron dust grain gyroradius is many 10's of R_e, the pickup region about the moon is expected to be very extended (gyroradius of $30R_e$ for 30 nm grains and $125R_e$ for 100 nm grains having perpendicular speeds of 3000 km/s). At the edges of this region, current conservation dictates the conversion of dust perpendicular currents into magnetic-field aligned currents that propagate into the northern and southern hemisphere (Goertz, 1980; Pontius and Hill, 1982, 2006; Saur et al., 2007). As described in Saur et al. (2007), it takes approximately 200 s for these parallel currents to propagate from Enceladus into the ionosphere. Currents launched from a small object will not close due to the corotational flow of the active field line past the object. However, for an extended pickup region (like that from dust), we might expect the field aligned currents to propagate to the ionosphere and back while a portion of the pickup region is still connected. Current closure would require a dust pickup region of ~ 30–$60R_e$ in extent in the X (corotation) direction which is comparable to the Enceladus dust cloud. Given the spatial extent of the dust pickup region, we should anticipate that the current loop is fully closed through the ionosphere, dissipating energy via Pedersen currents with a conductance of Σ_p. This ionosphere $J_\perp$ will then create a local $J_\perp \times B$ force that acts to slow the flux tubes connected to the dust pickup region.

The ambient saturnian magnetoplasma (no dust load) at 4 R_s will have an X-direction flow speed, U_o, of 39 km/s (in Saturn's frame of reference). However, the region of dust-created finite conductivity should act to shield the co-rotational E-field (E_o) and thus slow the plasma (Goertz, 1980; Pontius and Hill, 2006). Such a slow-down was indeed observed in the northern hemisphere dusty region between ~19:05–19:06:30 SCET. Fig. 1 shows the ratio of corotation-to-measured speeds, U_o/U, during the E3 Cassini Enceladus northern hemisphere transit as observed by the Langmuir Probe (LP) instrument on Cassini (Shafiq et al., 2011; Morooka et al., 2011). The U_o/U ratio exceeds a value of 5 during the northern hemisphere transit, suggesting a substantial slowdown to below 8 km/s near 19:06 SCET. This plasma velocity corresponds to an E-field inside the dusty region of 12% of the co-rotational value in exterior regions.

Simultaneous with the reduction in corotating plasma velocity (Tokar et al., 2009) is the sharp decrease in electron concentration which has been previously reported to be from dust absorption and collective dusty plasma effects (Farrell et al., 2009; Shafiq et al., 2011). Fig. 1 shows the associated ratio of the electron-to-ambient ion number density (n_e/n_o) inferred from the decrease in frequency of the upper hybrid resonance as measured by the Cassini RPWS (Farrell et al., 2009). The electron concentration decreased by almost a factor of 10 during the same time interval as the plasma slowdown. Assuming a dusty plasma system in charge equilibrium, we would expect the loss of plasma electrons to be compensated for by a corresponding increase in negatively charged grains (Shafiq et al., 2011), such that

$$\rho_i + \rho_e = \Delta\rho = -\rho_d \quad (2)$$

where the dust charged density, $\rho_d < 0$ and electron density, $\rho_e < 0$. The quantity $\rho_d(r)$ is the integral over the dust grain number density, $\int n_d(r) q_d(r) dr$. The overall measured dust particle size distribution at Enceladus has a steep variation with grain radius, varying as $r^{-4\ to\ -6}$ while the charge varies as $\sim r$ (Shafiq et al., 2011). Thus, it was concluded that the dominant dust charge density, ρ_d, associated with the electron dropout between 19:05 and 19:06 SCET is associated with submicron grains (<100 nm); those grains most susceptible to acceleration by the Lorentz force. We note that grains may be injected with no charge or with a surface-induced tribocharge (Jones et al., 2009) but will reach equilibrium with the plasma on time scales of hundreds of seconds, which is short compared to the acceleration times being considered herein (i.e., Fig. 1). For a local northern hemisphere ion current of 4×10^{-7} A/m^2 ($\sim$100/cm^3 at a flow velocity of 26 km/s), the equilibrium time for a 100 nm initially-negatively charged grain is ~750 s (using Eqs. (1) and (2) of Farrell et al. (2008)). For an electron thermal currents of 2×10^{-6} A/m^2 ($\sim$10/cm^3 at a 3 eV thermal velocity of $\sim 10^6$ m/s), the equilibrium time for a 100 nm positively charged grain is ~150 s.

We can then combine Eqs. (1) and (2) and derive a nominal grain radius, r_o, for Lorentz-accelerated grains consistent with both angular momentum and charge conservation. In essence, the dust's effect on the plasma can be 'inverted' to infer the submicron grain characteristics. To model the Enceladus dust current-to-ionosphere electrical connection, we assume that the region of dust-driven $J_\perp$ connects at its edges to magnetic field lines of infinite conductivity that carry the current parallel to B down to the saturnian ionosphere. The current closes across an ionosphere resistive load defined by the Pedersen conductance of $\Sigma_p \sim 0.1$ S (Pontius and Hill, 2006). We assume the dust current source, $J_\perp$, closes through the ionosphere in a way similar to Pontius and Hill (2006), such that the shielding E-field in the dust region varies as $\Delta E/E_o \sim \Sigma_d/(6\Sigma p + \Sigma_d)$. The plasma flow speed is $U = E_y/B_z$, and changes in cadence with the local $E \times B$ drift. We thus can define the dust conductance as

$$\Sigma_d = \Delta U\, 6\, \Sigma_p / U = \sigma_d L_z = \rho_d q_d \tau L_z / m_d \quad (3)$$

where ΔU is the difference between the corotation speed and that speed inside the high-conductivity region. ΔU is a Cassini-measured quantity. The right-hand side of the expression uses the conductivity value associated with Eq. (1), where ρ_d is also a Cassini-measured quantity determined via Eq. (2). We can now express the plasma-defined equilibrium charge on the grain as $q_d \sim \alpha(4\pi\varepsilon o \phi) r_o$, where ϕ is the dust grain potential (of −10 V herein) and α is a factor for icy-grain currents of ~3.7 (Shafiq et al., 2011). These q_d values are listed in Table 1. The icy grain mass varies as $m_d \sim 4\delta r_o^3$ where δ is the mass density of the ice particulate ($\delta \sim 1000$ kg/m^3). Substituting $q = q(r)$ and $m = m(r)$ into Eq. (3) and solving for the nominal grain radius, r_o, we find

$$r_o = (A \rho_d \tau L_z U / \Delta U\, 6\, \Sigma_p)^{1/2} \quad (4)$$

where A is a constant defined as $(\alpha\pi\varepsilon_o |\phi| \delta^{-1})$. The values of ρ_d, U, and ΔU are obtained directly from Cassini observations while A consists of constants. Fig. 1 shows the estimate of nominal pickup grain radius for various grain lifetimes (1000, 3160, and 10,000 s) using the observed Cassini values associated with the plasma slowdown and electron depletion. The calculations suggest that the accelerated grain sizes are between 50 and 200 nm. As suggested by Table 1, 50–200 nm grains are strongly coupled to the plasma environment via the Lorentz force.

3. Implications

While we focus herein on the Enceladus encounter on 12 March 2008 (the 'E3' encounter), there were a number of other north-to-south Cassini transits past Enceladus along similar trajectories as that shown in Fig. 1. Morooka et al. (2011) indicates that encounters E3–E6 each had similar characteristics: development of clear electron depletion and plasma slowdown that became very strong typically $5R_e$ northward of the moon. We thus infer that the northern hemisphere dust effect is a repeatable and quasi-time stationary structure. The northern electron density dropout and plasma slow-down was also stronger than the typical non-Enceladus E-ring passage. Wahlund et al. (2009) found that the plasma slows down by a factor of 2 during a typical E-ring crossings occurring at similar radial distances but azimuthally-displaced distant from the moon. However, the slow down and electron dropouts intensified significant during near-moon encounters (Morooka et al., 2011).

This particular result leads to a question: If the small-grain Lorenz dynamics occurs to immediately drive particles radially inward, how did the submicron particles get into the northern hemisphere in the first place? Jones et al. (2009) report on small grains (nanoparticles) present in the south pole geyser. Such southward directed particles would also become immediately influenced by the corotation E-field, transporting them in the +Y direction (radially-inward). Such grains would not easily migrate into the northern hemisphere region. As such, we suggest herein that the northern hemisphere submicron population is secondary ejecta; small fast grains associated with surface impacts by external, larger micron-sized dust grains. Such external micro-meteoid impactors could be from (1) E-ring grains in orbit at $4R_e$ (Spahn et al., 2006b), (2) high speed interplanetary dust (Spahn et al., 2006b), or

(3) grains originating from the moon's own plume (Kempf et al., 2010). In the last case, plume-originating micron-sized grains can migrate to northern hemisphere and impact the surface via gravitational forces (Kempf et al., 2010), to create smaller secondary impact ejecta. We note that secondary impact ejecta at initial velocities of a few hundred m/s will have grain lifetimes in excess of a few 1000 s in a region 1–3R_e in the northern hemisphere, consistent with the sizes and lifetimes considered in Fig. 1.

Fig. 2 shows a Monte Carlo model result of dust grain impact ejecta after 2000 s from a point source impact site. The source point is an example that is representative of a single impact release. Such releases occur impulsively everywhere over the sphere to form a moon-enveloping ejecta cloud (e.g., Fig. 1a of Spahn et al., 2006a). Fifty test particles were initially released with a Gaussian spread in negative v_y and positive v_z, with a velocity width of 500 m/s relative to the Enceladus. The test grain mass distribution had a peak at 4×10^{-18} kg (100 nm ice grain) and a distribution width of 2×10^{-18} kg. The forces on the grains in the model included the moon's gravity and the co-rotation E and B forces (with a grain surface potential of -10 V). Even though the ejecta was initially launched with a substantial $-v_y$ component, the corotation E-field redirected the submicron grains in the $+Y$ direction, creating a coherent dust $J_\perp$ that creates the $J_\perp \times B$ force. This $J_\perp$ is the 'pickup current' defined by Goertz (1980).

In the north region, the dust charge density $\rho_d \sim -10^{11}$ C/m^3 (Shafiq et al., 2011) and the plasma slowdown suggests a ~70–80% shielded E-field (at ~3.6 mV/m). The dust pickup velocity for a 100 nm grain after 2000 s is then $v_d \sim 700$ m/sec. We thus can estimate the dust current density, $J_y = \rho_d v_d \sim 7$ nA/m^2 in the northern hemisphere. Assuming this $J_\perp$ flows through a tube aligned with y of radius of 1R_e, we can estimate the dust current flowing along $-Y$ to be $I_\perp \sim 1500$ A in the northern hemisphere. Such a current flowing along $-Y$ should create a perturbation in B along the $-X$ direction at regions above the flow. Such a perturbation may have been reported by Dougherty et al. (2006), with an overflight of Enceladus in the northern hemisphere at >4R_e away from the moon revealing an unexpectedly large $-B_x$ perturbation in this hemisphere.

The effect of impact ejecta pickup may be occurring in the southern hemisphere as well. A model of the moon-enveloping impact ejecta cloud (without dust pickup) is shown in Fig. 1a of Spahn et al. (2006a). However, because of the addition of the intense plume ion pickup, discriminating between dust and ion pickup currents in the south is very difficult. The northern hemisphere region is thus a better dusty plasma laboratory, while the southern hemisphere ion plume dynamics adds another complication (i.e., another set of variables to isolate and solve). We leave the southern hemisphere pickup study for future work, and focus on the more pristine northern hemisphere herein.

To summarize, while the Cassini dust and radio instruments cannot directly detect the presence of the submicron grains in the northern hemisphere of Enceladus, we can infer their presence based on the macroscopic changes in the plasma, including the severe electron drop-out and the overall plasma slowdown in the northern hemisphere. While dust pickup is not a completely unique interpretation, it becomes difficult to devise another scenario to account for both the loss of electrons and simultaneous plasma slow-down.

References

Dougherty, M.K. et al., 2006. Identification of a dynamic atmosphere at Enceladus with the Cassini magnetometer. Science 311, 1406–1409.

Farrell, W.M. et al., 2008. Concerning the dissipation of electrically charged objects in the shadowed lunar polar regions. Geophys. Res. Lett. 35, L19104.

Farrell, W.M. et al., 2009. Electron density dropout near Enceladus in the context of water–vapor and water–ice. Geophys. Res. Lett. 36, L10203. doi:10.1029/2008GL037108.

Farrell, W.M. et al., 2010. Modification of the plasma in the near-vicinity of Enceladus by the enveloping dust. Geophys. Res. Lett. 37, L20202. doi:10.1029/2010GL044768.

Goertz, C.K., 1980. Io's interaction with the plasma torus. J. Geophys. Res. 85, 2949.

Gurnett, D.A. et al., 2004. The Cassini radio and plasma wave investigation. Space Sci. Rev. 114, 395. doi:10.1007/s11214-004-1434-0.

Hill, T.W., 1979. Inertial limit of corotation. J. Geophys. Res. 84, 6554.

Jones, G.H. et al., 2009. Fine jet structure of electrically charged grains in Enceladus' plume. Geophys. Res. Lett. 36, L16204. doi:10.1029/2009GL038284.

Kempf, S. et al., 2008. The E-ring in the vicinity of Enceladus: 1. Spatial distribution and properties of the ring particles. Icarus 193, 420. doi:10.1016/j.icarus.2007.06.027.

Kempf, S. et al., 2010. How the Enceladus dust plume feeds Saturn's E-ring. Icarus 206, 446–457.

Morooka, M.W. et al., 2011. Dusty plasma in the vicinity of Enceladus. J. Geophys. Res. 116, A12221. doi:10.1029/2011JA017038.

Pontius Jr., D.H., Hill, T.W., 1982. Departure from corotation of the Io plasma torus: Local plasma production. Geophys. Res. Lett. 9, 1321.

Pontius Jr., D.H., Hill, T.W., 2006. Enceladus: A significant plasma source for Saturn's magnetosphere. J. Geophys. Res. 111, A09214. doi:10.1029/2006JA011674.

Porco, C.C. et al., 2006. Cassini observes the active south pole of Enceladus. Science 311, 1393. doi:10.1126/science.11,23,013.

Saur, J., Neubauer, F.M., Schilling, N., 2007. Hemisphere coupling in Enceladus' asymmetric plasma interaction. J. Geophys. Res. 112, A11209.

Shafiq, M. et al., 2011. Characteristics of the dust–plasma interaction near Enceladus' South Pole. Planet. Space Sci. 59, 17–25.

Spahn, F. et al., 2006a. Cassini dust measurements at Enceladus and implications for the origin of the E-ring. Science 311, 1416. doi:10.1126/science.1121375.

Spahn, F. et al., 2006b. E ring dust sources: Implications from Cassini's dust measurements. Planet. Space Sci. 54, 1024–1032.

Tokar, R.L. et al., 2006. The interaction of the atmosphere of Enceladus with Saturn's plasma. Science 311, 1409. doi:10.1126/science.1121061.

Tokar, R.L. et al., 2009. Cassini detection of Enceladus' cold water-group plume ionosphere. Geophys. Res. Lett. 36, L13203. doi:10.1029/2009GL038923.

Wahlund, J.-E. et al., 2005. The inner magnetosphere of Saturn: Cassini RPWS cold plasma results from the first encounter. Geophys. Res. Lett. 32, L20S09. doi:10.1029/2005GL022699.

Wahlund, J.-E. et al., 2009. Detection of dusty plasma near the E-ring of Saturn. Planet. Space Sci. 57, 1795. doi:10.1016/j.pss.2009.03.011.

Waite Jr., J.H. et al., 2006. Cassini Ion and Neutral Mass Spectrometer: Enceladus plume composition and structure. Science 311, 1419. doi:10.1126/science.1121290.

Waite Jr., J.H. et al., 2009. Liquid water on Enceladus from observations of ammonia and 40Ar in the plume. Nature 460, 487. doi:10.1038/nature08153.

Young, D.T. et al., 2004. Cassini plasma spectrometer investigation. Space Sci. Rev. 114, 1. doi:10.1007/s11214-004-1406-4.